Compartmentalized Structure of the Plasma Membrane for Receptor Movements as Revealed by a Nanometer-level Motion Analysis

Yasushi Sako and Akihiro Kusumi

Department of Life Sciences, The University of Tokyo, Meguro-ku, Tokyo 153, Japan

Abstract. Movements of transferrin and α_2-macroglobulin receptor molecules in the plasma membrane of cultured normal rat kidney (NRK) fibroblastic cells were investigated by video-enhanced contrast optical microscopy with 1.8 nm spatial precision and 33 ms temporal resolution by labeling the receptors with the ligand-coated nanometer-sized colloidal gold particles. For both receptor species, most of the movement trajectories are of the confined diffusion type, within domains of $\approx$0.25 μm^2 (500–700 nm in diagonal length). Movement within the domains is random with a diffusion coefficient $\approx 10^{-9}$ cm^2/s, which is consistent with that expected for free Brownian diffusion of proteins in the plasma membrane. The receptor molecules move from one domain to one of the adjacent domains at an average frequency of 0.034 s^{-1} (the residence time within a domain $\approx$29 s), indicating that the plasma membrane is compartmentalized for diffusion of membrane receptors and that long-range diffusion is the result of successive intercompartmental jumps. The macroscopic diffusion coefficients for these two receptor molecules calculated on the basis of the compartment size and the intercompartmental jump rate are $\approx 2.4 \times 10^{-11}$ cm^2/s, which is consistent with those determined by averaging the long-term movements of many particles. Partial destruction of the cytoskeleton decreased the confined diffusion mode, increased the simple diffusion mode, and induced the directed diffusion (transport) mode. These results suggest that the boundaries between compartments are made of dynamically fluctuating membrane skeletons (membrane-skeleton fence model).

OUR understanding of the mechanisms that control localization, multimerization, and assembly of membrane proteins in the plasma membrane and their relationships with the membrane function is currently undergoing rapid evolution. Assembly of integral membrane proteins are key steps in the formation of special membrane domains such as coated pits, synapses, and cell-adhesion structures (Dubinsky et al., 1987; Pearse and Robinson, 1990). Oligomerization of integral membrane proteins and receptors are common occurrences in the plasma membrane (Kusumi and Hyde, 1982 and references therein; Ullrich and Schlessinger, 1990; Metzger, 1992), and in many cases are known to be involved in signal transduction in the plasma membrane, such as ligand-induced oligomerization of Fcγ, Fcϵ, and epidermal growth factor receptors. It has become clear that the non-homogeneous distribution and assembly of membrane proteins in the plasma membrane are, in part, regulated through the membrane-associated cytoskeleton, i.e., membrane skeleton. As a consequence, increasing attention has been directed toward understanding membrane-cytoskeleton interactions and their role in regulating the architecture of the plasma membrane (Bennett, 1990; Luna and Hitt, 1992). Of particular interest is the involvement of cytoskeletal elements in mediating or inhibiting assembly and aggregation of cell surface receptors, and their participation in the formation of specialized domains and in signal transduction in the plasma membrane.

One of the most useful ways to study interactions between the membrane and the cytoskeleton (and between membrane proteins) and to understand the mechanisms by which the localization and distribution of membrane proteins are regulatively varied is to monitor the movements of membrane proteins (Cherry, 1979; Kusumi et al., 1980; Kusumi and Hyde, 1982; Vaz et al., 1984; Jacobson et al., 1987; Edidin, 1987, 1990; Saxton, 1987, 1989*a*, *b*, 1990*a*, *b*; Abney et al., 1989; Edidin et al., 1991; Edidin and Stroynowski, 1991; Kusumi et al., 1993). In the case of the human erythrocyte membrane, observation of both lateral and rotational diffusion of band 3 in the spectrin network led Tsuji and coworkers to propose a spectrin dimer/tetramer equilibrium gate model (SPEQ gate model; Sheetz et al., 1980; Tsuji and Ohnishi, 1986; Tsuji et al., 1988). The mobile fraction of band 3 constitutes $\approx$80% of band 3 at 37°C (the immobile fraction of

Address all correspondence to Dr. Akihiro Kusumi, Department of Life Sciences, The University of Tokyo, Meguro-ku, Tokyo 153, Japan.

1. *Abbreviations used in this paper*: α2M, α_2-macroglobulin; α2M-R, α_2-macroglobulin receptor; FPR, fluorescence photobleaching recovery; MSD, mean square displacement; NRK, normal rat kidney fibroblastic cell; SPEQ gate model, spectrin dimer-tetramer equilibrium gate model; SPT, single particle tracking; Tf, transferrin; Tf-R, transferrin receptor.

band 3 [≈20%] is due to the binding of band 3 to the spectrin network via ankyrin). The rate of macroscopic diffusion of the mobile fraction of band 3 is determined by the "fence effect" of the spectrin tetramer network. Due to the steric hindrance produced by the spectrin meshwork to the passage of band 3 (the space between the membrane and the spectrin tetramer meshwork is too small for the cytoplasmic portion of band 3 to pass), the diffusion rate is limited by the frequency of band 3 to pass the spectrin fences, which in turn depends on the equilibrium between spectrin dimers (open gate, or broken fence) and tetramers (closed gate, or intact fence) (hence the term SPEQ gate model, also see Sheetz et al., 1980; Bennett, 1990; Saxton, 1989*b*, 1990*a*, *b*).

Recently, De Brabander and his colleagues and Sheetz and his colleagues have developed a technique for visualizing the movements of membrane receptors by labeling proteins with colloidal gold particles (20–40 nm in diameter) and observing the particles' movements on the living cell surface using video-enhanced contrast microscopy with nanometer spatial precision (single particle tracking, SPT or nanovid microscopy, De Brabander et al., 1985, 1986; Geerts et al., 1987, 1991; Gelles et al., 1988; Schnapp et al., 1988; Sheetz et al., 1989; Kucik et al., 1989; Qian et al., 1991; Cherry, 1992). The SPT method is unique in that it can reveal the mechanisms working on a single or a few protein molecules for regulating its (their) motion in the plasma membrane. The nanometer-level precision of SPT is particularly useful for studying regulation mechanisms that act at the submicron scale, such as the membrane skeleton (Kusumi et al., 1993). Methods for analyzing SPT data have been developed (Qian et al., 1991; Saxton, 1993; Kusumi et al., 1993).

In a previous report, we developed a method for classifying the trajectories observed by SPT into four types of motion; (1) stationary mode, (2) simple diffusion mode, (3) directed diffusion mode, and (4) restricted diffusion mode (or confined diffusion mode, in which a particle undergoing free diffusion is confined within a limited area) (Kusumi et al., 1993). Using this classification method and fluorescence photobleaching recovery (FPR), we investigated the mechanisms that regulate the movements of E-cadherin, epidermal growth factor receptor, and transferrin receptor (Tf-R) in both undifferentiated and differentiated mouse keratinocytes in culture. The results suggested that the plasma membrane is compartmentalized into small domains of 0.04–0.24 μm^2 (300–600 nm in diameter), as "felt" by the receptor molecules in the keratinocytes' plasma membrane.

These results were consistent with the "membrane-skeleton fence model" we proposed previously (Tsuji et al., 1988; Kusumi et al., 1993). This model proposes that the membrane-associated cytoskeleton (membrane skeleton) provides a barrier to free diffusion of membrane proteins due to the steric hindrance, thus compartmentalizing the membrane into many small domains for diffusion of integral membrane proteins. (The SPEQ gate model is a specific case of the membrane skeleton fence model in the human erythrocyte membrane.) The membrane proteins can escape from the compartments because of the dynamic properties of the membrane skeleton: the distance between the membrane and the skeleton may fluctuate over time, thus giving the membrane proteins some probability to pass the barrier, or the membrane-skeleton network may form and break continuously due to the dissociation-association equilibrium of the cytoskeleton.

In the present study, we have examined the movements of α_2-macroglobulin receptor (α2M-R) and transferrin receptor (Tf-R) in the plasma membrane of normal rat kidney (NRK) cells in culture with a spatial precision of 1.8 nm and a time resolution of 33 ms by using the SPT technique. The purpose of this work was threefold; (1) to investigate the molecular mechanism that controls the movements of these receptors on the cell surface, (2) to further characterize the compartmentalized structure of the plasma membrane by using these receptors as membrane probes, and (3) to contribute to clarify the mechanism by which these receptors are assembled to form coated structures (coated lattices and coated pits). De Brabander et al. (1988) previously studied the movements of Tf-R in A431 cells using the colloidal-gold probe technique, and examined the endocytotic pathways of Tf-R on the cell surface as well as in the cytoplasm. However, nanometer-level analysis of these movements was not performed.

Approximately 80% of both receptor molecules showed confined-diffusion-type movements. Quantitative analysis of the trajectories indicated that (*a*) the plasma membrane is compartmentalized into many small domains of ≈0.25 μm^2 with regard to diffusion of these receptors in the membrane, (*b*) the receptor molecules move from one domain to an adjacent domain an average of once every 29 s, (*c*) within a domain, the receptor molecules undergo rapid lateral diffusion that is indicative of free diffusion within a compartment (≈10^{-9} cm^2/s), (*d*) the rate of long-range diffusion of these receptors is determined by the size of the compartment and the frequency of jumps between compartments, and (*e*) partial destruction of the microfilaments or microtubules dramatically changes the motional modes of these receptors, with the destruction of microfilaments having the greater effect.

Materials and Methods

Conjugation of Tf and α_2M to Gold Particles

Gold particles of 20 and 40 nm in diameter were prepared as described previously (De Mey, 1983; Leunissen and De Mey, 1986; Kusumi et al., 1993). A suspension of gold particles (5 ml) was centrifuged at 8,000 *g* for 30 min and the loose pellet was resuspended in 2 ml of 2 mM citrate-phosphate buffer (pH 7.0), and then mixed with either 50 μl of 25 mg/ml bovine holo Tf (Wako, Tokyo) or 0.5 ml of 5 mg/ml bovine α_2-macroglobulin (α2M, Boehringer, Indianapolis, Indiana) in citrate-phosphate buffer. After incubation on ice for 1 h, 200 μl of 10% BSA was added to the suspension and the mixture was further incubated for 1 h. The suspension was centrifuged at 8,000 *g* for 30 min and the pellet was resuspended by sonication for 10 s in 2 ml of HBSS buffered with 10 mM Hepes (pH 7.4) containing 1% BSA (HBSS-BSA). The excess ligands were removed by repeating centrifugation and resuspension in HBSS-BSA five times. The centrifugation period was prolonged to 70 min for 20-nm gold particles. α2M on the gold particles was activated by incubation with 0.5 ml of 1 M methylamine for 1 h (Ashcom et al., 1990). The conjugates were sterilized by filtration with 0.22 μm filters and stored at 4°C.

Cell Cultures and Gold Labeling

A NRK fibroblast cell line was routinely cultured in a minimum essential medium supplemented with nonessential amino acids and 10% FBS. Cells used for microscopic observation were cultured on 18 mm × 18 mm coverslips (No. 1) for 2 d after plating. The cells on a coverslip were washed with

ice-cold HBSS twice, cooled on ice for 10 min, and then incubated with a 60-μl suspension of ≈1.5-nM gold particles conjugated with the receptor ligands on ice for 45 min. Preparations for microscopy were made by inverting the coverslip with the cells and the gold suspension on a microscope slide glass using strips of adhesive tape (≈0.15-mm thick) as spacers. Microscopic observation was made in the presence of excess amounts of gold particles in the medium (no washing was performed). The medium was perfused by hand every 10 min. For observation of receptor movements for ≈6 min, the cells on the cover glass were completely sealed to prevent water evaporation.

Specificity of the binding of the colloidal gold particles to the receptor molecules was examined by incubating the cells at 4°C with ≈1.5-nM gold particles in the presence of a 100-fold excess amount of the free ligands (both were added simultaneously). The cells were then fixed and examined by video-enhanced microscopy. As another control, binding of gold particles that were coated only with BSA to the cells was examined.

Drug Treatments

Cells were preincubated with the culture medium containing 1 μM of cytochalasin D (Sigma Chem. Co., St. Louis, MO) or 2 μM of vinblastin (Sigma) for 2 h before incubation with the gold particle suspension. The observation was carried out in the presence of the same concentration of the drugs.

Video Microscopy

Video-enhanced differential interference contrast microscopy was used to observe cells and the movements of gold particles attached to the receptor molecules in the plasma membrane of living cells (Kusumi et al., 1993). A Zeiss Axioplan microscope was equipped with an oil-immersion condenser lens (NA = 1.4) and an oil-immersion Plan-Neofluar objective (63×, NA = 1.4 or 100×, NA = 1.3). The temperature of the sample was maintained at 37 ± 1°C by covering the microscope with a specially designed plastic chamber and controlling the temperature with a Nikon temperature controller (model NP-2). Illumination was provided through an optical fiber (Technical Video, Woodshole, MA) using the green line (wavelength = 546 nm) of a 100-W mercury arc lamp (HBO100). The image was projected through two intermediate lenses (total magnification of 3.2-4×) on a Hamamatsu CCD camera (C2400-77, Hamamatsu, Japan). Real-time mottle subtraction and contrast enhancement were achieved by a Hamamatsu DVS-3000 image processor and the processed image was recorded on a Panasonic TQ-3100F laser disk recorder. For short-term observations, 500 video frames (= 16.7 s) were recorded in a sequence. For long-term observations, time-lapse recording of every 333 ms was carried out for ≈6 min.

Quantitative Measurements of the Movements of Colloidal Gold Particles

Positions (x and y coordinates) of the selected gold particles were determined automatically by a computer program that employs the method developed by Gelles et al. (1988). The video images were digitized with a DVS-3000 and the selected area of the image was sent to a computer (via IEEE 488, an IBM-PC compatible Intel 486 machine). The accuracy of the position measurement was estimated by recording a sequence of 150 video frames of the images of a 40-nm gold particle fixed on a polylysine-coated coverslip and impregnated in 10% polyacrylamide gel. The standard deviation of the coordinates of the fixed particles was 1.8 nm horizontally and 1.4 nm vertically, which is comparable to the published values (Gelles et al., 1988; Schnapp et al., 1988). The nominal diffusion coefficient of the fixed particle was 3.2×10^{-13} cm^2/s, which, therefore, is the lower limit for determination of the diffusion coefficient with the present setting.

Calculation of the Mean-Square Displacement from the Trajectories of Gold Particles

For each trajectory of a particle, the mean-square displacement (MSD), $\langle(\Delta r(\Delta t))^2\rangle$, for every time interval (Eq. 1) was calculated according to the formula (Gross and Webb, 1988; Lee et al., 1991; Qian et al., 1991; Kusumi et al., 1993):

$$\mathrm{MSD}(n\delta t) = 1/(N-1-n)\sum_{j=1}^{N-1-n}\{[x(j\delta t+n\delta t)-x(j\delta t)]^2 + [y(j\delta t+n\delta t)-y(j\delta t)]^2\}, \quad (1)$$

where δt is the video frame time (33 ms) and $(x(j\delta t + n\delta t), y(j\delta t + n\delta t))$ describes the particle position following a time interval $\Delta t_n = n\delta t$ after starting at position $(x(j\delta t), y(j\delta t))$, N is the total number of frames in the video recording sequence, n and j are positive integers, and n determines the time increment.

Results

Labeling of α2M-R and Tf-R with Colloidal Gold Particles on the Cell Surface

NRK cells were incubated with a suspension of 1.5 nM gold particles conjugated with transferrin (Tf, 40-nm gold particles) or α_2-macroglobulin (α2M, 20-nm gold particles) at 4°C for labeling of Tf-R or α2M-R, respectively, on the cell surface. The cells were observed at 37 ± 1°C in the presence of 1.5-nM gold particles by video-enhanced differential interference contrast microscopy. Gold particles were continually attached to the membrane surface, and then internalized by endocytosis. The steady-state number of gold particles located on the cell surface under these conditions was approximately 100/cell (Fig. 1 *a*). These particles were scattered over the entire cell surface. This binding was inhibited (to

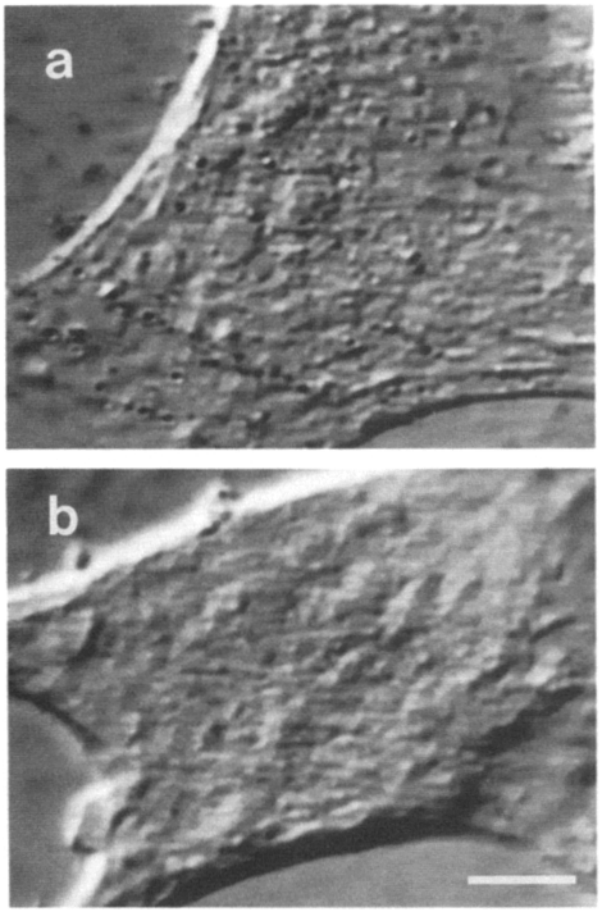

Figure 1. Video-enhanced differential interference contrast images of colloidal-gold labeled NRK cells. The cells were incubated with 1.5 nM Tf-coated colloidal gold particles in the absence (*a*) and presence (*b*) of 5 mg/ml Tf on ice for 3 h. The cells were then washed with HBSS and fixed with 2% paraformaldehyde on ice for 10 min. The bar indicates 10 μm.

only several particles/cell) by incubation with the gold particles in the presence of a 100-fold excess amount of the free ligands (which was premixed with the gold particles before addition to cells) at 4°C at which internalization of receptors does not take place (Fig. 1 *b*). This result suggests that these gold particles behave as individual ligand molecules (Mecham et al., 1991). Gold particles that had been coated only with BSA did not bind to the cells (a few particles/cell).

Clathrin-coated structures (coated lattices + coated pits, Miller et al., 1991) occupy ≈2% of the membrane area in NRK cells, as determined by electron microscopy and by indirect immunofluorescence staining using anti-clathrin antibodies (data not shown). Electron microscopy according to the method of Aggeler et al. (1983) and Miller et al. (1991) showed that ≈5% of the gold particles that are attached to Tf-R are located in coated structures in the steady state (data not shown, Takeuchi et al., 1992). However, during observation by video-enhanced microscopy, we were unable to tell which particles were actually in the coated structures. Since many endosomes containing Tf-gold and α2M-gold particles were observed inside the cells, which agrees with the observation by De Brabander et al. (1986), we do not think the gold particles that are attached to the receptors inhibit the receptors' entry into the coated pits.

The movements of the attached gold particles on the surfaces of living cells were investigated. The position of each particle was determined frame by frame using the method developed by Schnapp et al. (1988). The spatial precision for determining the horizontal and vertical coordinates was 1.8 and 1.4 nm, respectively, for 40-nm gold particles fixed on a coverslip.

Long-Range Diffusion of Receptor Molecules in the Plasma Membrane: Compartmentalized Structure of the Plasma Membrane

Long-term movements of receptor molecules were observed by time-lapse recording for ≈6 min at a rate of 3 video frames/s (Fig. 2). Particles that stayed on the cell surface throughout the observation period were used for analysis. Typical trajectories of the movements of gold particles attached to Tf-R and α2M-R are shown in Fig. 2 (*A* and *B*). The trajectories suggest that diffusion of these receptors are not simple Brownian. Qualitatively, the receptors diffuse rapidly within a confined domain, which we call a "membrane compartment" or a "membrane domain", of ≈0.5 μm (diameter). The receptors occasionally move out of the domain into one of the adjacent domains and undergo rapid diffusion within the new domain. Long-range diffusion of receptor molecules appears to occur by successive jumps from one domain to adjacent domains.

In Fig. 2, the membrane compartments were qualitatively

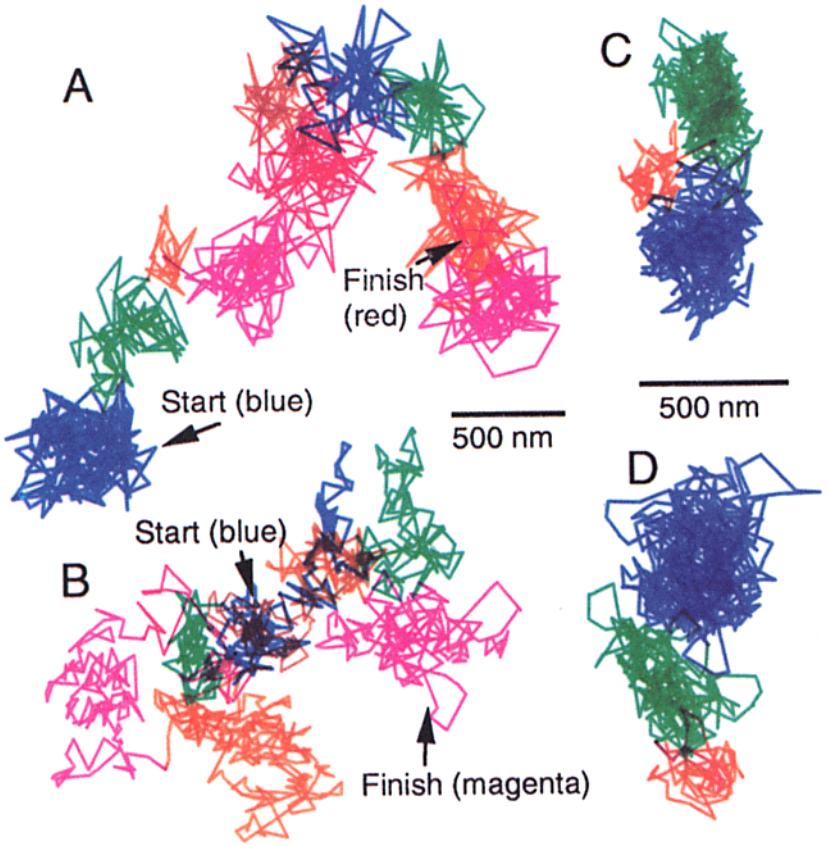

Figure 2. Typical long-term trajectories (≈6 min) of Tf-R in the plasma membrane of the NRK cells. Observation was made using time-lapse video recordings (*A*, *B*; 3 video frames/s, 1,000 frames). The x and y coordinates of the particle were determined in each video image, and the successive coordinates are connected by straight lines. By following the trajectories closely by eye, plausible compartments (*domains*) were found, and are shown in different colors. The particles move in the following colored domains: blue - green - orange - magenta - red - brown - and back to blue to start the next round. Tf-R molecule is (*B*) often returned to compartments that it had passed through previously, i.e., blue and brown, green and red, orange and a second blue. Although examination of this nature is qualitative, it suggests approaches to quantitative analysis. Since these time-lapse recordings have sparse points, short-term trajectories were recorded at the normal video rate, which indicate similar domains (*C* and *D*, ≈20 s). The bar indicates 500 nm.

Many trajectories of particles undergoing simple Brownian diffusion, at first sight, may look similar to these trajectories. For example, see Fig. 1.4 in "Random Walks in Biology" by Berg (1983), which shows a trajectory generated by computer simulation. Rigorous distinction has to wait for statistical examination, as is shown later (Kusumi et al., 1993). However, distinction between the tendency of Brownian particles to stay in the same place (and to move to the next dwell position) and the trajectories shown here is quite clear even by eye examination. The characteristics of these trajectories which distinguish themselves from simple Brownian cases are (1) the adjacent domains are always closely apposed to each other, and (2) the ratio of the domain size versus the step size is considerably smaller than that in simple Brownian trajectories.

determined by following each trajectory very closely by eye, and each plausible compartment is shown in a different color. The particles occasionally returned to a compartment that they had passed through previously via several other compartments. For example, see the trajectory *B* in Fig. 2. These results suggest that each compartment may be stable for more than a few minutes. Since these are time-lapse recordings, the points may look too sparse. In Fig. 2, trajectories for shorter periods but recorded at the normal video rate are also shown (trajectories *C* and *D*). These trajectories also suggest confined diffusion and intercompartmental hop diffusion.

Since these trajectories cannot by themselves speak to confined diffusion, rigorous statistical examination is required, which is given later in this report. (Such movement is statistically possible for particles undergoing Brownian motion. However, qualitatively, since these trajectories are typical for almost all long-term trajectories of Tf-R and α2M-R, it is unlikely that they are all explained by the simple Brownian diffusion.) The major reason that we are showing these trajectories in the early part of this paper is to give the readers a good idea on the subject matter. In addition, although these trajectories by themselves do not prove hop diffusion of receptors between membrane compartments, the other side of the logic is that if the model for hop diffusion in the compartmentalized membrane is correct (Fig. 7), the trajectories *must* look like the ones shown in Fig. 2.

Based on such eye examination of the trajectories, approximate center-to-center distances between adjacent compartments (L_{cc}) and the residence time in each compartment (τ_{LT} where LT indicates long-term observation) were estimated. The distributions of L_{cc}(LT) and τ_{LT} are shown in the histograms in Fig. 3, respectively. Short-term trajectories such as those shown in Fig. 2 (*C* and *D*) can also be used in the estimation of L_{cc} (L_{cc}(ST), where ST indicates short-term observation, (Table I). The mean values of L_{cc} obtained from both long-term and short-term trajectories are 550 nm and 400 nm for Tf-R and α2M-R, respectively (Table I). The average values of τ_{LT} are 36 s and 27 s for Tf-R and α2M-R, respectively. (The frequency of jump from one compartment to an adjacent compartment is the inverse of the residence time in each compartment.) These results suggest that the long-range diffusion of membrane receptors in the plasma membrane, such as that observed by FPR, takes place via intercompartmental receptor movements. In fact, if the receptors are strictly confined to the compartments,

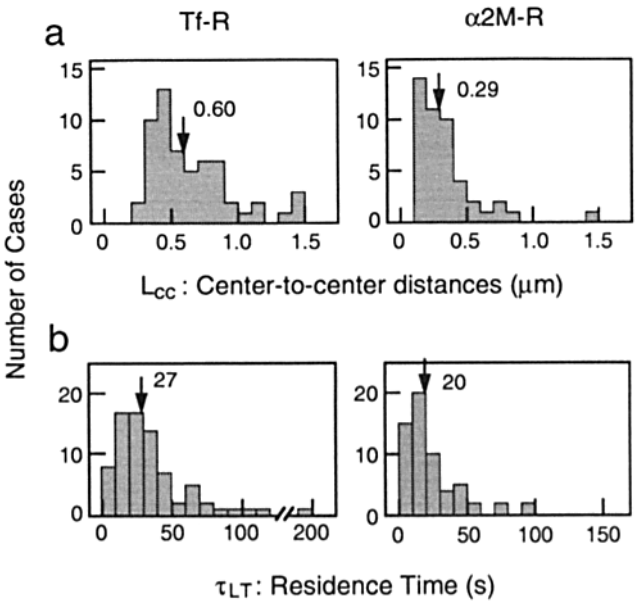

Figure 3. Histograms showing the distribution of L_{cc} (*a*: center-to-center distances between adjacent compartments, a measure of the compartment size) and τ_{LT} (*b*: residence time within a compartment) as estimated from the long-term trajectories. The arrows indicate the median values.

then receptor molecules cannot assemble into coated pits. We would like to caution the readers again that these dwell times (τ_{LT} and τ_{ST}) and domain sizes (L_{cc}) are determined subjectively. However, in the discussion related to Fig. 6 and Table IV (L_{cc} and L_r) and Fig. 8 (τ's; in addition, τ_{calc} in Table I is thoroughly explained), we will come back to this point and show that these estimates match well with the data obtained by quantitative and statistical analyses of receptor trajectories.

None of the trajectories for ≈6 min indicated any sign of directed diffusion (toward the coated pits). This result suggests that the assembly of receptors occurs by random diffusion and entrapment at the coated pit or cooperative formation of the pit via interaction with adaptor complexes and clathrin, and not by lipid flow or by transport by the cytoskeleton.

The long-term trajectories shown here may be interpreted as the movement of diffusing receptors within connected

Table I. Center-to-Center Distances (L_{cc}) between Two Adjacent Compartments and the Residence Time (τ) of the Receptors in a Single Compartment Estimated in Various Ways

Receptors	L_{cc} (LT)	L_{cc} (ST)	L_{cc} (mean)	τ_{LT}	τ_{ST}	τ (mean)	τ_{calc}
	nm	*nm*	*nm*	*s*	*s*	*s*	*s*
Tf-R	660 ± 310 (58)	350 ± 170 (31)	550 ± 310 (89)	36 ± 29 (77)	27 (29)	34 (106)	15
α2M-R	340 ± 250 (46)	460 ± 280 (37)	400 ± 270 (83)	27 ± 22 (62)	16 (37)	23 (99)	23

L_{cc}(LT), L_{cc}(ST), and L_{cc}(mean) indicate the center-to-center distances of the domains estimated from long-term and short-term trajectories, and their weighted average, respectively. The data are shown as the mean ± SD, and SD includes both experimental error and the true distribution. τ_{LT} is estimated from the long-term trajectories by simple eye examination. τ_{ST} is the total observation time for short-term trajectories divided by the total number of jumps observed during this time +1. τ (mean) is the weighted average of τ_{LT} and τ_{ST}. τ_{calc} is estimated from the macroscopic diffusion coefficient (Table III and Fig. 8) and the confined area size (Table IV). See the text that comments on Fig. 8 for details. Numbers in parentheses for L_{cc}'s indicate the total number of observed intercompartmental jumps during this study, those for τ_{LT}'s indicate the total number of observed compartments, and those for τ_{ST}'s indicate the total number of observed intercompartmental jumps during the total observation time of short-term trajectories.

lipid-rich domains in the plasma membrane, which is crowded with membrane proteins. However, we do not think this likely because the adjacent compartments are often found to be closely apposed to each other (i.e., lying side by side with a fairly clear boundary line in-between them, Fig. 2, *C* and *D*).

Quantitative Analysis of Receptor Movement

Quantitative characterization of the receptor movements was carried out by analyzing the trajectories for 500 video frames (16.7 s) with a time resolution of 33 ms (video frame time). Since the residence time of each receptor molecule within a domain is ≈30 s (Table I), the trajectories during a 16.7-s period are likely to reflect movement within 1–3 compartments (mostly 1 compartment). The trajectories of most particles in this time range are characterized by rapid, random movement within small regions (Fig. 2, *C* and *D*). Even during this short period of time, some particles move out of the original region and into adjacent regions. Directed transport-like motion was rarely observed (1 out of 72 and 70 particles for Tf-R and α2M-R, respectively).

Quantitative analysis of the x and y particle positions with time was carried out to obtain more information about the movements of receptors and their control mechanisms. Plotting the mean-square displacement of the particle as a function of the time interval (Δt),

$$MSD(\Delta t) = \langle (x(t) - x_0)^2 + (y(t) - y_0)^2 \rangle \quad (2)$$

yields simple and informative representation of data (Fig. 4, Sheetz et al., 1989; Lee et al., 1991; Zhang et al., 1991; De Brabander et al., 1991; Qian et al., 1991; Kusumi et al., 1993). (x(t), y(t)) and (x_0, y_0) are the positions of the particle at measurements separated by a time interval Δt and $\langle \ldots \rangle$ indicates an average over one trajectory. In general, a sequence of 90 averaged steps (i.e., averaged movements for Δt = 3 s) was produced from a sequence of 500 video frames.

Three modes of receptor motion can be distinguished from the MSD-Δt plot: (1) simple Brownian diffusion mode, (2) confined diffusion mode, and (3) directed diffusion mode.

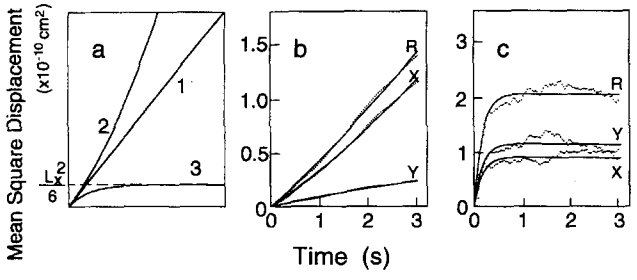

Figure 4. MSD-Δt plots for diffusing particles. (*a*) Theoretical curves for simple Brownian diffusion (1), directed diffusion (2), and confined diffusion (3) are shown for one-dimensional diffusion (x direction). The graphs are drawn assuming that D's are identical for all cases (the slope at time 0 is $2D_x$). (*b–c*) Typical MSD-Δt plots for simple diffusion (*b*; $D = 0.68 \times 10^{-11}$ cm²/s) and confined diffusion (*c*; $D = 6.74 \times 10^{-11}$ cm²/s, $L_x = 237$ nm, $L_y = 267$ nm). X, Y, and R indicate diffusion in x and y directions and in a two-dimensional plane, respectively.

The characteristics of these diffusion modes and the essence of theory are summarized below (see Kusumi et al., 1993, for details).

(1) Simple Brownian diffusion mode. The MSD-Δt plot (Fig. 4: *a-1* and *b*) is linear with a slope of 4D ($2D_x$ and $2D_y$ for x and y directions, respectively), and can be expressed as:

$$MSD_x(\Delta t) = 2D_x\Delta t,\ MSD_y(\Delta t) = 2D_y\Delta t \quad (3)$$
$$MSD(\Delta t) = 4D\Delta t \quad (4)$$
$$4D = 2D_x + 2D_y \quad (5)$$

where D is the 2-dimensional diffusion coefficient, and D_x and D_y are 1-dimensional diffusion coefficients for x and y directions, respectively (see curve *1* in Fig. 4 *a*). A typical MSD-Δt plot for simple Brownian case is shown in Fig. 4 *b*:

(2) Confined diffusion mode, in which a receptor molecule undergoes Brownian diffusion within a limited area and cannot move out of the area during the time interval ($0 \leqslant x \leqslant L_x$, $0 \leqslant y \leqslant L_y$). Intuitively, this mode can occur when a receptor molecule is trapped within a membrane domain that is enclosed by the cytoskeleton/membrane skeleton (membrane skeleton fence model), or when a receptor molecule is tethered to a loose cytoskeleton (without any restoring potential, i.e., the spring constant is 0) that can be extended up to a length of $\approx(L_x^2 + L_y^2)^{1/2}$. (By "loose cytoskeleton", we mean flexible parts of the cytoskeleton, such as an end portion of a thin actin fiber which is not involved in actin bundles or actin meshwork.) The short-term trajectories used for quantitative analysis cannot differentiate between these two models. However, the observation of long-term diffusion shown in Fig. 2 indicates that the former model is correct.

The mathematical expression of MSD-Δt plot is given in Kusumi et al. (1993). The slope of the curve at time 0 is again $2D_x$ and $2D_y$ and the diffusion coefficient reflects that within a compartment (Fig. 4, *a3*). The curve asymptotically approaches $L_x^2/6$ and $L_y^2/6$ in the x and y directions, respectively.

(3) Directed diffusion mode (transport mode), in which a protein molecule moves in a direction at a constant drift velocity v_x (v_y), with superimposed random diffusion with a diffusion coefficient D_x (D_y). The MSD-Δt plot is parabolic with a differential coefficient of 4D at time 0 (initial slope, see curve 2 in Fig. 4 *a*). Tf-R and α2M-R did not show this mode in NRK cells in the intact state (i.e., before treatments with cytochalasin D or vinblastin).

The diffusion coefficients, transport velocity, and/or the confined area were obtained by curve fitting of the MSD-Δt plots using the equations described in Kusumi et al. (1993). Fitting was carried out by least squares analysis using the Gauss-Newton procedure.

The diffusion coefficients D determined by SPT reflect those at the nanometer level. Since it is proportional to the slope (differential coefficient) at Δt = 0 in the MSD-Δt plot, it can be determined independently of the motional modes (Fig. 4 *a*). In contrast, the diffusion coefficients determined by FPR reflect macroscopic diffusion in the membrane at scales larger than a micrometer. Since the latter coefficients are influenced by both the viscosity properties of the membrane at the nanometer level and the membrane structures at the micrometer level, they cannot differentiate between these two effects. Thus, the diffusion coefficient obtained by

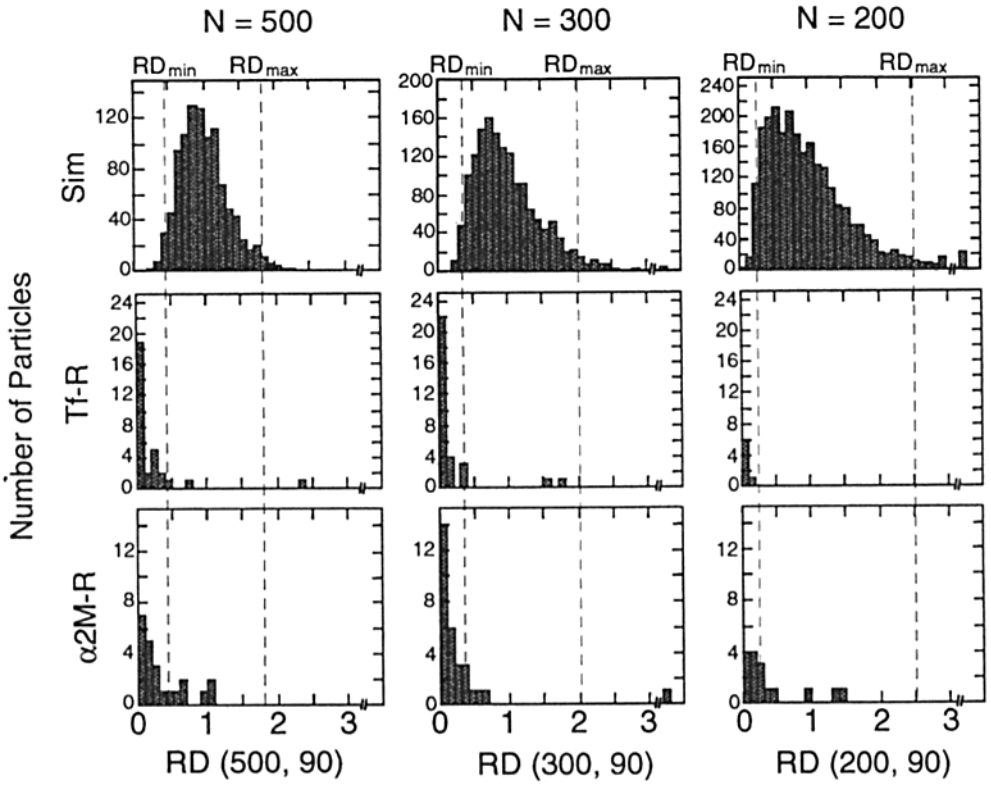

Figure 5. Histograms showing relationship between the number of particles and RD(N, 90). *N* values employed were 500, 300, and 200 and Δt = 3 s, i.e., 90 steps. $RD_{min}(N, 90)$ and $RD_{max}(N, 90)$, as determined from the distribution of RD(N, n) for simulated Brownian particles (*Sim*: *top row*), are shown by vertical broken lines. The total number of simulated particles was 1,000, 1,500, and 2,000 for *N* = 500, 300, and 200, respectively. The experimental data are shown in the middle (*Tf-R*) and bottom (*α2M-R*) figures. Note that the distributions for experimental particles are completely different from that for simulated particles, for which simple Brownian diffusion was assumed.

SPT is referred to as "microscopic diffusion coefficient" in this paper to distinguish it from that determined by FPR.

Classification of the Motional Modes

Classification of each trajectory into one of the three modes of motion described above was carried out by the method we developed previously (see Materials and Methods and Kusumi et al., 1993 for details). The parameter that was used to describe relative deviations from ideal Brownian diffusion, RD, was defined as $MSD(\Delta t)/4D\Delta t$, and the theoretical distribution of RD for free Brownian diffusion was obtained by performing a computer simulation of the movements of Brownian particles. A duration of 3 s (90 video steps) was used as the time interval (Δt) (Kusumi et al., 1993). Fig. 5 (*top row*, Sim) shows a histogram of the number of simulated Brownian particles versus RD. In the case of simple diffusion, the average RD should be ≈1. For the confined and directed diffusion modes, RD should be smaller and larger than 1, respectively.

RD values that give 2.5 percent of the particles from both ends of the distribution, referred to as RD_{min} and RD_{max}, were determined, and are shown by vertical broken lines in Fig.5. When the trajectory of an experimental particle showed an RD value larger than RD_{max} or smaller than RD_{min}, it was classified as having a directed or confined diffusion mode, respectively.

It should be noted here that the present method of classification is based on the exclusion of the hypothesis of simple diffusion. Therefore, the number of particles exhibiting the simple diffusion mode is overestimated. The limiting area size and transport velocity that are detectable and sufficient for classification into the confined or directed diffusion modes, respectively, depend on the microscopic diffusion coefficient. The pertinent relationships are summarized in Kusumi et al. (1993).

Similar histograms for experimental particles attached to Tf-R and α2M-R are shown in Fig. 5 (*middle* and *bottom rows*, respectively). To examine the dependence of the MSD-Δt plot on the total number of frames in a video recording sequence (N) (since the probability of intercompartmental jump increases with N), N was varied (500, 300, and 200 steps; with Δt = 3 s, i.e., n = 90 steps, see Eq. 1 in Materials and Methods section). The data obtained from 72 and 70 trajectories of Tf-R and α2M-R, respectively, are shown. The shapes of the histograms for experimental particles are quite different from those for simulated Brownian particles, and the peaks are shifted toward smaller RD values, which indicates that most experimental particles are undergoing confined diffusion.

Table II shows the fraction of Tf-R and α2M-R in each motional mode. Approximately 85% of Tf-R and 75% of α2M-R show the confined diffusion mode. Almost no directional movements were observed, indicating the absence of bulk membrane flow or transport of these receptor mole-

Table II. Motional Modes (%) for Tf-R and α2M-R in NRK Cells

Receptors	Simple diffusion	Confined diffusion	Directed diffusion
	%	%	%
Tf-R	13	86	1
α2M-R	24	75	1

Classification is based on a statistical test that a given trajectory has less than a 2.5% probability of having the simple Brownian diffusion mode.

Table III. Microscopic and Macroscopic Diffusion Coefficients for Tf-R and α2M-R (×10⁻¹⁰ cm²/s ± SD) Determined by SPT

Receptors	Microscopic D* (×10⁻¹⁰ cm²/s)			Macroscopic D* (×10⁻¹⁰ cm²/s)	
	Simple diffusion	Confined diffusion	Directed diffusion	Jump+size‡ (+ simple diffusion§)	MSD-Δt‖
Tf-R	1.1 ± 0.90 (9)	7.0 ± 7.9 (62)	0.40 (1)	0.14 (0.27)	0.32
α2M-R	2.0 ± 2.13 (17)	9.1 ± 10.7 (52)	0.59 (1)	0.34 (0.75)	0.34

The numbers in parentheses for the microscopic D indicate the number of gold particles observed. SD includes both experimental error and the true distribution of the diffusion coefficient.
* "D" indicates diffusion coefficient in this table.
‡§‖ The macroscopic diffusion coefficient determined ‡from the intercompartmental jump rate and the size of the compartment (and averaged with the simple diffusion mode with the weight determined from the mode classification§) and ‖that from the average MSD-Δt plot in Fig. 8. See the subsection "Macroscopic Diffusion of Receptors in the Plasma Membrane" for details.

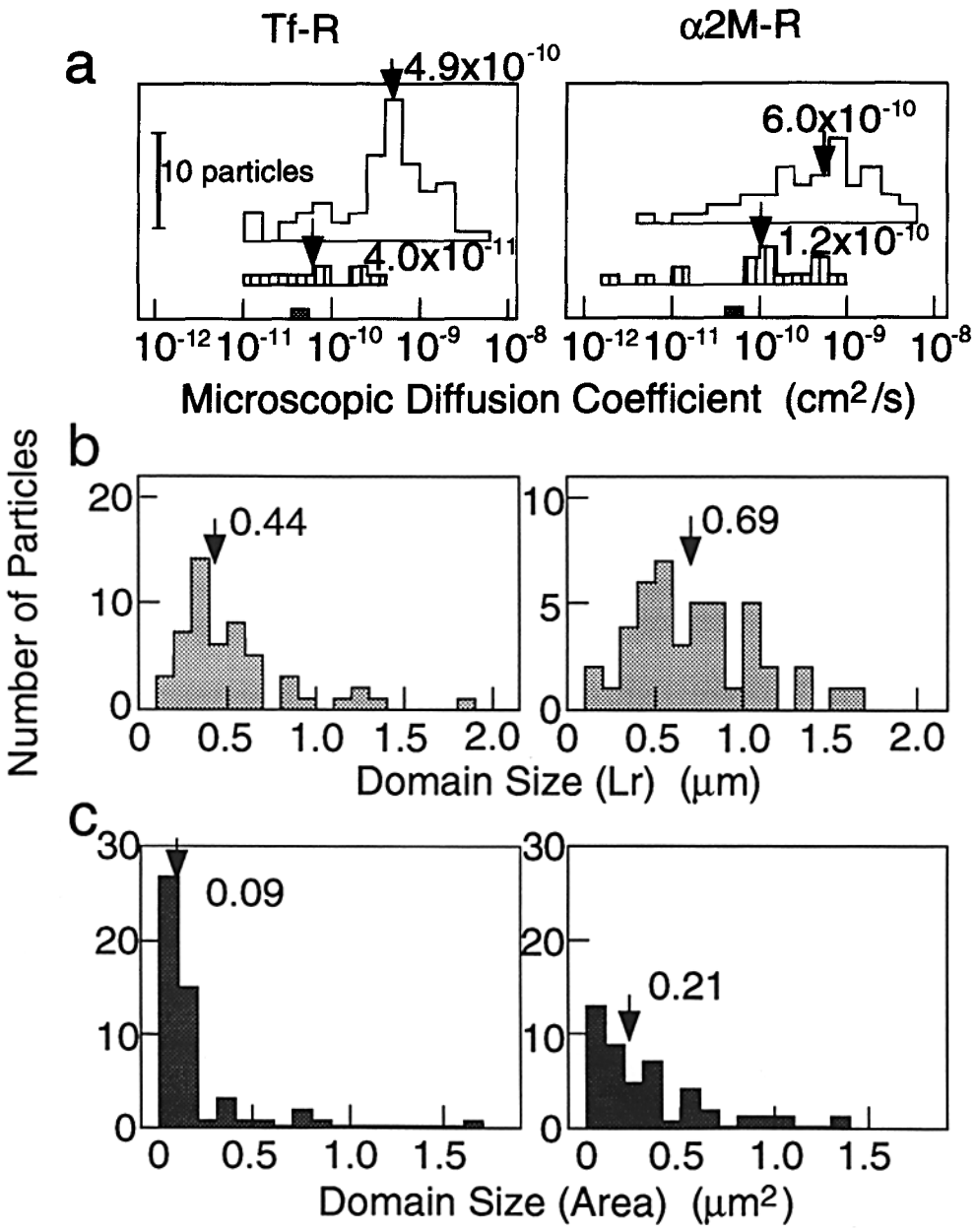

Figure 6. Histograms showing the number of particles vs the microscopic diffusion coefficient (a) and the compartment size (*b* and *c*). (*a*) Microscopic diffusion coefficient is shown for each diffusion mode: *open*, confined diffusion; *stripes*, simple diffusion; *hatched*, directed diffusion. (*b* and *c*) The distribution of the compartment size determined from the confined diffusion mode: L_r (*b*: the diagonal distance = $(L_x^2 + L_y^2)^{1/2}$) and the domain size (*c*: L_xL_y in μm^2). The arrows indicate the median value for each distribution.

cules by the cytoskeleton. These results agree with those from the long-term observation of particles shown in Fig. 2.

Microscopic Diffusion Coefficients

Table III summarizes the mean values for microscopic diffusion coefficients for the three diffusion modes. Fig. 6 *a* shows histograms of the microscopic diffusion coefficient for each receptor in each motional mode. The general tendency is that D for the confined diffusion mode is larger than D for the simple diffusion mode. The histograms of D for confined diffusion appear to consist of two components. This distinction is clearest in the case of Tf-R: D for the slow component is similar to that for the simple diffusion mode, while that for the fast component is larger than $\approx 10^{-10}$ cm²/s. If we apply this classification, then the average D's are 4.8 ($\pm$2.7) $\times$ 10^{-11} cm²/s for the slow component (28%) and 8.2 ($\pm$8.0) $\times$ 10^{-10} cm²/s for the fast component (72%) for the Tf-R (averaged over all modes). This distinction is less clear for α2M-R.

The slow component may be due to the binding to cytoskeleton, coated structures, or to other proteins that are undergoing slow diffusion. Further discussion on this point will be given later.

Previously, we found that the microscopic diffusion coefficient for Tf-R in the plasma membrane of the mouse keratinocyte cell line (F7p) is 4–8 $\times$ 10^{-11} cm²/s on average, substantially smaller than those found in NRK cells in the present study (Kusumi et al., 1993). We examined several other cell lines including CHO cells, chick embryonic fibroblastic cells, and mouse fibroblastic L cells. D's obtained ranged between 10^{-9} and 10^{-10} cm²/s (unpublished observations). The reason for this large cell-dependent variation has not been clarified. Factors such as variation in the amount of trapped Tf-R in the clathrin-coated structures, local mobilities, and the extent of crowdedness in the membrane, and binding to loose cytoskeletal filaments that can be dragged in long distances are being considered.

Motional Characteristics of the Confined Diffusion Mode

Most ($\approx$80%) of Tf-R and α2M-R in the plasma membrane of NRK cells undergo confined diffusion. The size for the confining compartment in each case was obtained by fitting the curves in the MSD-Δt plot using Eqs. 11–13 in Kusumi et al. (1993). Histograms for the compartment sizes are shown in Fig. 6, *b* and *c*. Each compartment averaged over both Tf-R and α2M-R has a mean diagonal length ($L_r = [L_x^2 + L_y^2]^{1/2}$) of 620 nm and a mean area (L_xL_y) of 0.25 μm² (Table IV). The compartments are nearly isotropic in shape. These characteristics for the size and shape of the compartments are similar for both receptors, suggesting that the compartment reflects characteristics of the membrane rather than of individual receptor species. By definition L_r may be slightly larger than L_{cc}, which is the center-to-center distance between adjacent domains estimated by eye examination (Table I; $L_r \approx 1 - 1.4 \times L_{cc}$). Actually 530 nm vs 550 nm for Tf-R and 730 nm vs 400 nm for α2M-R were observed for L_r vs L_{cc} (Tables I and IV), which indicates quite good agreement.

The average residence time of receptor molecules within a compartment was obtained by dividing the total observation time (the sum of the short-term observation times) by the total number of intercompartmental jumps (+1) that were detected in the short-term trajectories by eye examination (τ_{ST}). τ_{ST}'s for Tf-R and α2M-R are 27 and 16 s, respectively (Table I). These numbers are comparable to those determined from the long-term observation of receptor diffusion, as shown in Fig. 2 (τ_{LT}'s for Tf-R and α2M-R are 36 and 27 s, respectively. See Table I and Fig. 3).

The microscopic diffusion coefficients for Tf-R and α2M-R molecules that exhibit the confined diffusion mode are $\approx 10^{-9}$ cm²/s (Fig. 6 *a* and Table III). The diffusion coefficients reflect those within compartments. These values are independent of the presence of the barriers because they are calculated from the initial slope near $\Delta t = 0$ in the MSD-Δt plot.

These microscopic diffusion coefficients for Tf-R and α2M-R molecules that are undergoing confined diffusion are thought to be similar to the diffusion coefficient for proteins undergoing free diffusion in lipid-protein membranes (percolation diffusion in the presence of mobile obstacles, Saxton, 1987). The diffusion coefficient for rhodopsin in the rod outer segment disk membrane in the frog retina is $\approx 4 \times 10^{-9}$ cm²/s (Poo and Cone, 1974), which, to our knowledge, is the largest diffusion coefficient ever reported for transmembrane proteins in biological membranes. Rhodopsin molecules are believed to diffuse freely in these membranes without interacting with the cytoskeleton. The protein-to-lipid ratio in the disk membrane is $\approx$1/60, which may explain the slower diffusion of rhodopsin in rod outer segment membranes than that expected for proteins reconstituted in lipid-rich membranes (Peters and Cherry, 1982; Kusumi and Hyde, 1982).

These results, together with those in Fig. 2 and Table I, suggest that long-range diffusion occurs by repeated intercompartmental movements of receptor molecules. The slow diffusion coefficients observed for integral membrane proteins by FPR are mainly due to the time needed to cross the domain barriers and not due to slow diffusion at the nanometer-level. Dependence of the diffusion rate on the size of the bleaching (and observation) area in FPR experiments

Table IV. The Compartment Size (the Confined Area) as Estimated from the Short-Term Trajectories of Particles That Were Classified as Exhibiting the Confined Diffusion Mode

Receptors	L_r	Area	Anisotropy (R)	n*
	nm	*μm^2*		
Tf-R	530 $\pm$ 330	0.19 $\pm$ 0.28	1.4 $\pm$ 0.3	52
α2M-R	730 $\pm$ 360	0.31 $\pm$ 0.30	1.4 $\pm$ 0.5	45
mean	620	0.25	1.4	97

L_r = diagonal length = $(L_x^2 + L_y^2)^{1/2}$ (nm). Area = L_xL_y (μm^2). Shape anisotropy of the compartment (R) = $L_i/L_j (L_i > L_j)$. The data are shown as the mean $\pm$ SD, and SD includes both experimental error and the true distribution. *n* is the number of particles. L_x and L_y were obtained by curve fitting (Fig. 4).

* *n*'s in this table are smaller than those in Table III (62 and 52). While mode classification was carried out using a 2-dimensional diffusion model, L_x and L_y were obtained on the basis of 1-dimensional analysis, and they do not always converge for both x and y directions. This occurs when the shape of the compartment is extremely anisotropic, e.g., L_x = 0.1 μm and L_y = 2 μm. In contrast, note that the microscopic D's can be determined for all particles from the initial slope in the MSD-Δt plot.

(Yechiel and Edidin, 1987; Edidin and Stroynowski, 1991) is consistent with this conclusion. Since most particles exhibit the confined diffusion mode, we propose that the observed compartmentalized structure is a basic feature of the plasma membrane.

Characteristics of Movements in the Simple Diffusion Mode

The microscopic diffusion coefficients for particles undergoing simple diffusion are generally smaller than those for particles undergoing confined diffusion (by a factor, on average, of ≈6 for both receptor species studied here, Fig. 6 *a*, Table III). It is likely that the particles undergoing slow diffusion tend to have a lower probability of colliding with the domain boundaries during the observation period. Hence, their trajectories tend to be classified as simple diffusion.

In the case of confined diffusion, an interplay among D, the time interval (Δt), and the size of the confined domain ($L_x L_y$) should be noted. Due to the relationship $\langle r^2 \rangle = 4D\Delta t$, as the size of the domain increases, the domain is increasingly more difficult to detect for constant D and Δt. Since a particle with D = 10^{-8} cm²/s, ≈ the maximum D value observed in this work, will cover an area of 10 μm^2 during 3 s (90 steps), the present method can only detect membrane domains comparable to or smaller than 10 μm^2. As D decreases, the particles have less probability to "feel" the boundaries of the domain. For D = 10^{-11}–10^{-10} cm²/s, the particles will cover an area of only 0.01–0.1 μm^2 (100–300 nm square) during 3 s (n = 90 steps). In addition, since the statistics we used here were designed to unequivocally identify the non-Brownian diffusion modes (at a risk factor of 2.5%), most of the particles that show intermediate behavior between Brownian and non-Brownian particles are classified as Brownian particles (Using this method, we were conservative in our classification of the confined diffusion mode, which is the major subject of this study).

We propose (1) that the compartmentalized structure (possibly due to the membrane-skeleton fence) is a basic feature of the plasma membrane, (2) that particles which are classified as exhibiting the simple diffusion mode, ≈20% of all particles, are undergoing "apparently simple diffusion", and (3) that such particles are located in large compartments and/or have small microscopic diffusion coefficients. Particles undergoing fast diffusion tend to collide with the membrane-skeleton fence more often, but those undergoing slower diffusion or which are located in larger compartments have less of a chance to "sense" the boundaries. Therefore, "simple diffusion" is simply an operational term in this experimental approach, and the readers are cautioned to be careful about the semantics.

Absence of the Stationary Mode for Tf-R and α2M-R

There has been no previous report on the mobility of receptors in clathrin-coated structures. However, it is believed that receptors within coated structures are tightly packed and immobile (Pearse and Crowther, 1987). Although we were unable to determine which particles were actually in coated structures under the video optical microscope (≈5% of gold particles conjugated with Tf are localized in the coated structures), one of the major characteristics of the histograms of the microscopic diffusion coefficient shown in Fig. 6 *a* is the absence of the stationary mode, as defined in our previous report (Kusumi et al., 1993). According to the previous method, particles with diffusion coefficients smaller than 3 × 10^{-12} cm²/s were classified as having the stationary mode. All of the particles examined in this study, except one, showed diffusion coefficients greater than 4.6 × 10^{-12} cm²/s, and moved in an area larger than 0.01 μm^2 (in the case of confined diffusion), while the smallest diffusion coefficient that can be measured with our instrument is ≈4 × 10^{-13} cm²/s.

We raise a possibility that the receptors in coated structures are still somewhat mobile, and merely show small D and/or confinement area. This may explain the two peaks in the histograms of the microscopic diffusion coefficient for the confined diffusion mode (particularly for TR in Fig. 6 *a*), i.e., the slow component may be due to entrapment in coated structures. (The possibility also exists that the plasma membrane, including the membrane skeleton and coated structures, is undergoing large thermal fluctuation, which increases apparent diffusion coefficients for stationary receptors.)

Macroscopic Diffusion of Receptors in the Plasma Membrane

The data for short-term diffusion shown in Figs. 4 and 5 and Table IV indicate that, for a period of ≈29 s (Table I), the receptor molecules are confined within a 0.25 μm^2 domain and undergo rapid diffusion within the confined area. The long-term observations of trajectories shown in Fig. 2 and Table I indicate that long-range diffusion occurs by successive movements of receptors from one compartment to another, as shown in the model in Fig. 7. In this model, the *macroscopic* diffusion coefficient is determined not by the microscopic diffusion coefficient, but by the frequency of intercompartmental jumps and the size of each compartment. Based on the average jump rate between compartments

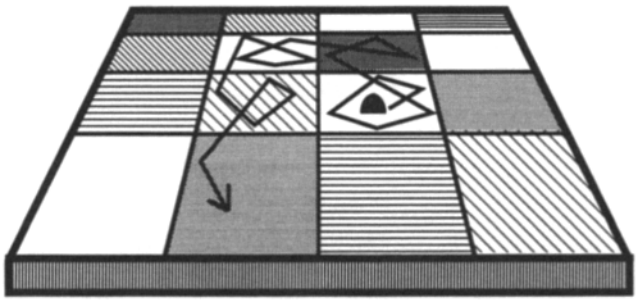

Figure 7. A model showing the compartmentalized structure of the plasma membrane. The plasma membrane is compartmentalized into many domains of 0.2–0.3 μm^2 for diffusion of both receptor molecules. The receptor molecules undergo almost free diffusion within a domain (slowed only by the presence of other membrane proteins), to which they are confined for an average of ≈29 s. The receptor molecules move from one compartment to one of the adjacent domains at a frequency of ≈0.034 s^{-1} (2 min^{-1}), on average, and the long-range diffusion of receptors is the result of successive intercompartmental movements. Therefore, the *macroscopic* diffusion rate is determined from the size of the compartment and the frequency of jumps between compartments, and gives the macroscopic D of ≈ 2.4 × 10^{-11} cm²/s.

(=average inverse residence time in a compartment = $1/\tau$ (mean) = 0.0294 and 0.0435 s^{-1} for Tf-R and α2M-R, respectively, from Table I; note that these numbers were determined by eye examination of trajectories and somewhat subjective) and the average compartment size (0.19 and 0.31 μm^2 for Tf-R and α2M-R, respectively, from Table IV), the macroscopic diffusion coefficients were estimated to be 1.4 $\times$ 10^{-11} cm^2/s for Tf-R and 3.4 $\times$ 10^{-11} cm^2/s for α2M-R (Table III). If we account for the presence of the simple diffusion mode, the overall macroscopic diffusion coefficients are calculated to be 2.7 $\times$ 10^{-11} cm^2/s and 7.5 $\times$ 10^{-11} cm^2/s for Tf-R and α2M-R, respectively (Table III).

The macroscopic diffusion coefficients can also be estimated from the long-term trajectories, such as those shown in Fig. 2. MSD's for long-term diffusion were calculated and averaged for 24 Tf-R and 16 α2M-R molecules. The MSD's averaged over many independent trajectories (as opposed to averaging over a single trajectory as in Fig. 4) are plotted against time in Fig. 8. The most important characteristic in these plots is that MSD increases linearly with time (except near $t = 0$), which indicates simple Brownian diffusion. No sign of confined diffusion can be detected in these plots after averaging over only ≈20 molecules, i.e., the motional characteristics of the individual receptor molecules are completely lost after averaging. This result clearly indicates the importance of observing the receptor movements at the level of single (or a small number of) molecules for studying the mechanism of receptor movements, assembly, and localization.

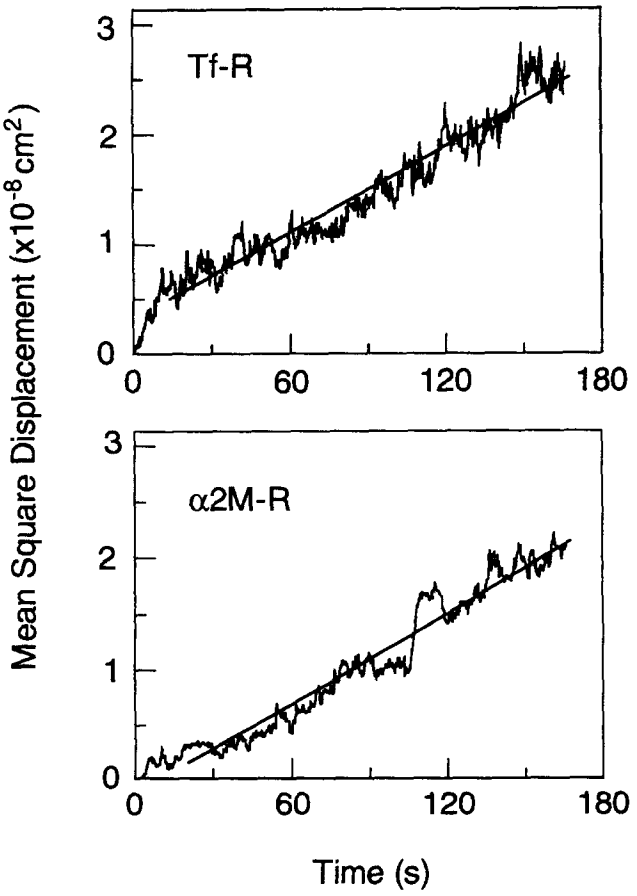

Figure 8. The relationships of MSD vs t obtained by ensemble averaging for movements of Tf-R and α2M-R during 170 s. After averaging only ≈20 trajectories, all of the features of confined diffusion were lost, which indicates the importance of observing individual molecules. The square-displacements of 24 (*a*, Tf-R) and 16 (*b*, α2M-R) independent trajectories were averaged rather than averaging over a single trajectory, as in Fig. 4 (Eq. 1). By fitting these data to a linear function, macroscopic diffusion coefficients of 3.2 and 3.4 $\times$ 10^{-11} cm^2/s were obtained for Tf-R and α2M-R, respectively (fitted for t = 10 − 167 s; see Table III).

The macroscopic diffusion coefficients evaluated from the slope of the MSD-time plots in Fig. 8 are 3.2 $\times$ 10^{-11} cm^2/s and 3.4 $\times$ 10^{-11} cm^2/s for Tf-R and α2M-R, respectively (Table III). These values are close to the diffusion coefficients determined from the frequency of intercompartmental jumps and the compartment size (see Table III).

In the previous argument, the intercompartmental jump rate was determined somewhat subjectively. However, since we now have a good estimate of the macroscopic diffusion coefficients (as above, Table III) and the domain size (Area in Table IV), which were determined independently and without using the subjective dwell time within a domain, we can evaluate the intercompartmental jump rate assuming a model shown in Fig. 7. The dwell time (τ_{calc}) within a compartment determined in this way is 15 and 23 s for Tf-R and α2M-R, respectively (Table I), which agree reasonably well with τ_{LT} and τ_{ST}. These results indicate consistency in various analysis methods used in the present study.

We were unable to determine whether the diffusion coefficients estimated here are consistent with those obtained by FPR, since FPR data are not available for these receptor molecules. Our attempt to measure FPR on these receptors was unsuccessful due to rapid internalization of these receptor molecules. The fluorescence signal from the internalized receptors prevented the measurement of lateral diffusion on the cell surface. Meanwhile, FPR data have been reported for a few other receptors involved in endocytosis. The diffusion coefficients for the mobile fraction of epidermal growth factor receptor (EGF-R) (Livneh et al., 1986) and asialoglycoprotein receptor (Heins et al., 1990) are 2.3 $\times$ 10^{-10} cm^2/s with 49% immobile fraction and 10^{-10} cm^2/s with 40% immobile fraction, respectively. These diffusion coefficients are 3–10 times larger than those obtained here. This difference may be due to the use of a large probe (20–40 nm ϕ) in SPT. However, direct comparison of FPR data with the present data is somewhat difficult because of the presence of large fractions of immobile components in FPR results (which is not present in SPT results). Molecules with slow hopping rate between compartments or those confined longer in some of the compartments will be classified into the immobile fraction in FPR, while these types of molecules will be considered slowly diffusing in SPT display, which would greatly reduce the average diffusion coefficient in SPT measurements for macroscopic diffusion (Kusumi et al., 1993). In addition, the receptor species are different. Therefore, we refrain from further comparison and speculation in the present paper.

The Effects of Partial Destruction of the Cytoskeleton on Receptor Movements

Actin filaments and microtubules were partially destroyed by

Table V. Motional Modes (%) of Tf-R and α2M-R after Treatment with 1 μM Cytochalasin D or 2 μM Vinblastin

Receptors	Treatment	Simple diffusion	Confined diffusion	Directed diffusion
		%	%	%
Tf-R	Control	13	86	1
	Cytochalasin D	50	23	27
	Vinblastin	45	44	11
α2M-R	Control	24	75	1
	Cytochalasin D	57	29	14
	Vinblastin	28	64	8

Classification is based on a statistical test that a given trajectory has less than a 2.5% probability of being a simple Brownian diffusion case.

Table VI. The Average Microscopic Diffusion Coefficient ($\times 10^{-10}$ cm²/s) Tf-R and α2M-R after Treatment with 1 μM Cytochalasin D or 2 μM Vinblastin

Receptors	Treatment	Simple diffusion	Confined diffusion	Directed diffusion
		($\times 10^{-10}$ cm²/s)	($\times 10^{-10}$ cm²/s)	($\times 10^{-10}$ cm²/s)
Tf-R	Control	1.1 ± 0.90 (9)	7.0 ± 7.9 (62)	0.40 (27)
	Cytochalasin D	0.13 ± 0.15 (51)	0.77 ± 2.8 (23)	0.09 ± 0.08 (27)
	Vinblastin	0.76 ± 1.1 (34)	0.61 ± 0.80 (33)	0.74 ± 1.1 (8)
α2M-R	Control	2.0 ± 2.1 (17)	9.1 ± 10.7 (52)	0.59 (1)
	Cytochalasin D	0.18 ± 0.12 (56)	0.61 ± 1.5 (29)	0.11 ± 0.06 (14)
	Vinblastin	1.4 ± 3.2 (21)	1.7 ± 2.4 (49)	0.04 (6)

The numbers in the parentheses indicate the number of particles. SD includes both experimental error and the true distribution of the diffusion coefficient.

treating cells with 1 μM cytochalasin D and 2 μM vinblastin, respectively. SPT indicated that treatment with cytochalasin D induced a large decrease in the confined diffusion mode and an increase in the simple diffusion mode, and generated a large fraction for the directed diffusion mode (27 and 14% for Tf-R and α2M-R, respectively (Table V), although almost none of the receptors displayed this mode before the treatment. Many cytoskeletal filaments were still present after the treatment.) Microscopic diffusion coefficients for the confined and simple diffusion modes decreased greatly (Fig. 9 *a* and Table VI). Accordingly, the apparent domain size decreased (since only smaller domains are detectable for particles undergoing slower diffusion, Table VII and Fig. 9 *b*), and the fraction of particles that were classified operationally into the simple diffusion mode increased (Table V). Similar effects were observed after treatment with vinblastin, but the extent of the effect tended to be smaller. These results agree with the cytochalasin B-induced effect on polylysine-coated

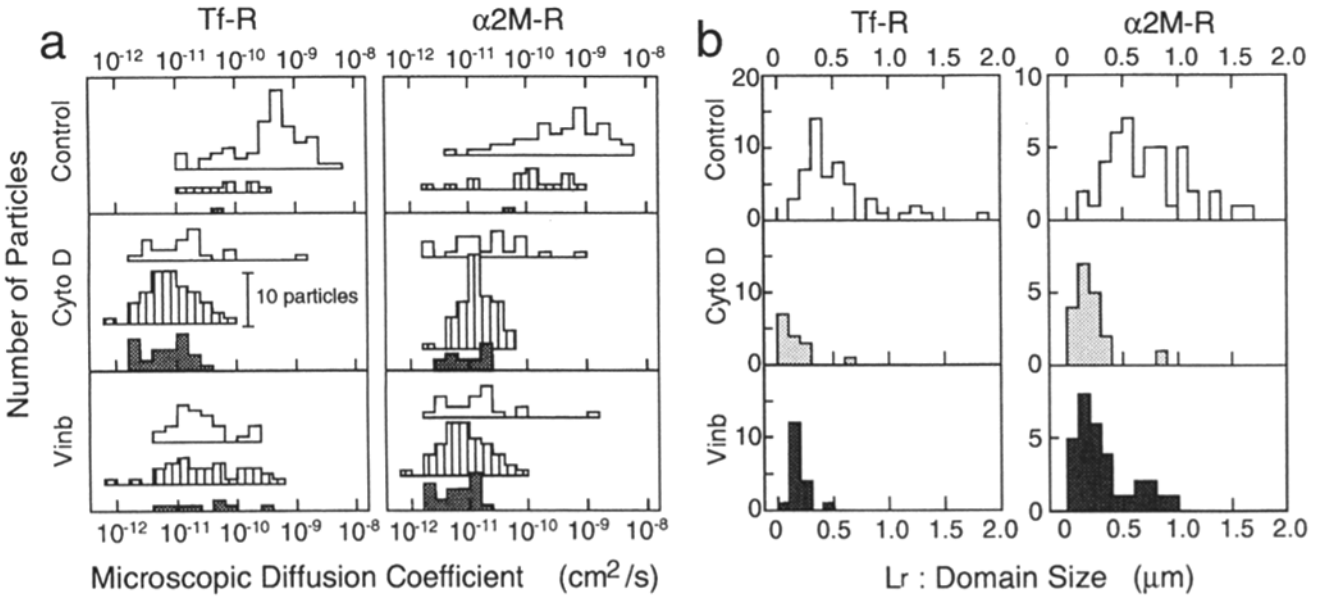

Figure 9. Histograms showing (*a*) the number of particles vs the microscopic diffusion coefficient and (*b*) the number of particles vs L_r (the diagonal length of the compartment) after treatment with 1 μM cytochalasin D or 2 μM vinblastin. Keys for (*a*): *open*, confined diffusion; *stripes*, simple diffusion; *hatched*, directed (transport type) diffusion.

Table VII. The Average Compartment Size (L_r and area) for TF-R and α2M-R after Treatment with 1 μM Cytochalasin D or 2 μM Vinblastin

Particles	Treatment	L_r (μm) average	L_r (μm) median	Area (μm²) average	Area (μm²) median	Anisotropy (R)	n
Tf-R	Control	0.53 ± 0.33	0.46	0.19 ± 0.28	0.092	1.4 ± 0.3	52
	Cytochalasin D	0.16 ± 0.15	0.14	0.02 ± 0.05	0.006	1.5 ± 0.3	15
	Vinblastin	0.21 ± 0.13	0.16	0.03 ± 0.04	0.012	1.7 ± 0.7	18
α2M-R	Control	0.73 ± 0.36	0.69	0.31 ± 0.30	0.210	1.4 ± 0.5	45
	Cytochalasin D	0.22 ± 0.16	0.21	0.04 ± 0.07	0.017	1.5 ± 0.3	19
	Vinblastin	0.33 ± 0.24	0.28	0.07 ± 0.10	0.029	1.8 ± 0.8	31

n = the number of particles. SD includes both experimental error and the true distribution.

gold particles on PtK_2 cell surfaces (De Brabander et al., 1991). We speculate that when the collapse and aggregation of the cytoskeleton were induced, the receptor molecules were entrapped within the collapsed membrane skeleton.

Discussion

Movements of transferrin and α2-macroglobulin receptor molecules in the plasma membrane of cultured NRK cells were investigated. For both receptor species, the movements of ≈80% of the receptor molecules are confined within compartments of ≈0.25 μm² (500–700 nm in diagonal length). The movements inside the compartments are random with a diffusion coefficient ≈10^{-9} cm²/s, which is consistent with that expected for free Brownian diffusion of proteins in the plasma membrane. The receptor molecules move from one compartment to an adjacent compartment at a frequency of 0.034 s^{-1} (the average residence time in each compartment is ≈29 s). The macroscopic diffusion coefficients calculated on the basis of the domain size and the intercompartmental jump rate are ≈2.4 × 10^{-11} cm²/s, which is consistent with those determined by averaging the long-term movements of many particles. This view of the movements of membrane receptors agrees with the intuitive impression obtained from the long-term trajectories, such as those shown in Fig. 2. Since the quantitative analysis of short-term trajectories alone cannot differentiate between the "confinement in a cage" model and the "tethering with a rope" model, observation of long-term trajectories was important. When a receptor-gold complex is captured with a laser optical tweezer and dragged back and forth in the plane of the membrane, the complex often escapes from the trap at the same place regardless of the direction of the movement (Sako, Y., and A. Kusumi, unpublished data). These results are readily explained by the membrane-skeleton fence model, but not by the tethering model.

These results are also in accord with our previous observation of movements of epidermal growth factor receptor, Tf-R, and E-cadherin in the dorsal (apical) plasma membrane of keratinocytes (F7p) in culture (Kusumi et al., 1993). The average size of the domains in these cells is ≈400 nm diagonally.

In the present study with NRK cells, some particles (≈20%) were shown to exhibit the simple Brownian diffusion mode, but the diffusion coefficient is smaller by a factor of 6–10 as compared with those displaying the confined diffusion mode, which suggests that these particles do not experience domain boundaries during the observation period because they do not collide with the boundaries due to the small diffusion rate within the domain. In this sense, the simple diffusion mode as defined operationally here is simply a matter of semantics. It is concluded that compartmentalization into domains, such as that shown in the model in Fig. 7, is a basic feature of the plasma membrane. The long-range diffusion of receptors is the result of the successive intercompartmental movements.

We speculate that the compartment boundaries consist of a membrane-skeleton/cytoskeleton fence structure, which is present throughout the cytoplasmic surface of the plasma membrane, except in special functional domains such as coated pits and cell adhesion structures. In these functional domains, other underlying structures such as clathrin-coated structures and desmosomal plaques are present on the cytoplasmic surface.

Small fractions of both receptors showed slow microscopic diffusion coefficients smaller than 10^{-10} cm²/s in both simple Brownian and confined diffusion modes. It is possible that these fractions represent the receptor molecules bound to the cytoskeleton/membrane-skeleton or to the coated structures. Further results on the slow component will be published elsewhere.

The present data suggest involvement of the membrane skeleton in the control of protein organization and localization in the plasma membrane via compartmentalization of the plasma membrane. It would be necessary to rethink the mechanisms that control localization, oligomerization, and assembly of the plasma membrane proteins on the basis of the compartmentalized structure by the membrane skeleton.

References

Abney, J. R., B. A. Scalettar, and J. C. Owicki. 1989. Self diffusion of interacting proteins. *Biophys. J.* 55:817–833.

Aggeler, J., R. Takemura, and Z. Werb. 1983. High-resolution three-dimensional views of membrane-associated clathrin and cytoskeleton in critical-point-dried macrophages. *J. Cell Biol.* 97:1452–1458.

Ashcom, J. D., S. E. Tiller, K. Dickerson, J. L. Cravens, W. S. Argraves, and D. K. Strickland. 1990. The human α_2-macroglobulin receptor: identification of a 420-kD cell surface glycoprotein specific for the activated conformation of α_2-macroglobulin. *J. Cell Biol.* 110:1041–1048.

Bennett, V. 1990. Spectrin-based membrane skeleton: a multipotential adaptor between plasma membrane and cytoplasm. *Physiol. Rev.* 70:1029–1065.

Berg, P. 1983. Random Walks in Biology. Princeton University Press, Princeton, NJ. p. 12.

Cherry, R. J. 1979. Rotational and lateral diffusion of membrane proteins. *Biochim. Biophys. Acta.* 559:289–327.

Cherry, R. J. 1992. Keeping track of cell surface receptors. *Trends Cell Biol.* 2:242–244.

De Brabander, M., G. Geuens, R. Nuydens, M. Moeremans, and J. De Mey. 1985. Probing microtubule-dependent intracellular motility with nanometre

particle video ultramicroscopy (Nanovid ultramicroscopy). *Cytobios.* 43:273–283.

De Brabander, M., R. Nuydens, H. Geerts, and C. R. Hopkins. 1988. Dynamic behavior of the transferrin receptor followed in living epidermoid carcinoma (A431) cells with nanovid microscopy. *Cell Motil. Cytoskeleton.* 9:30–47.

De Brabander, M., R. Nuydens, G. Geuens, M. Moeremans, and J. De Mey. 1986. The use of submicroscopic gold particles combined with video contrast enhancement as a simple molecular probe for the living cell. *Cell Motil. Cytoskeleton.* 6:105–113.

De Brabander, M., R. Nuydens, A. Ishihara, B. Holifield, K. Jacobson, and H. Geerts. 1991. Lateral diffusion and retrograde movements of individual cell surface components on single motile cells observed with nanovid microscopy. *J. Cell Biol.* 112:111–124.

De Mey, J. 1983. Colloidal gold probes in immunocytochemistry. *In* Immunocytochemistry (practical applications in pathology and biology). J. M. Polak and S. van Noorden, editors. Wright PSG, Bristol. 83–112.

Dubinsky, J. M., D. J. Loftus, G. D. Fischbach, and E.L. Elson. 1989. Formation of acetylcholine receptor clusters in chick myotubes: migration or new insertion? *J. Cell Biol.* 109:1733–1743.

Edidin, M. 1987. Rotational and lateral diffusion of membrane proteins and lipids: phenomena and function. *Curr. Top. Membr. Trans.* 29:91–127.

Edidin, M. 1990. Molecular associations and membrane domains. *Curr. Top. Membr. Trans.* 36:81–96.

Edidin, M., and I. Stroynowski. 1991. Differences between the lateral organization of conventional and inositol phospholipidanchored membrane proteins. A further definition of micrometer scale domains. *J. Cell Biol.* 112: 1143–1150.

Edidin, M., S. C. Kuo, and M. P. Sheetz. 1991. Lateral movements of membrane glycoproteins restricted by dynamic cytoplasmic barriers. *Science (Wash. DC).* 254:1379–1382.

Geerts, H., M. De Brabander, R. Nuydens, S. Geuens, M. Moeremans, J. De Mey, and P. Hollenbeck. 1987. Nanovid tracking: a new automatic method for the study of mobility in living cells based on colloidal gold and video microscopy. *Biophys. J.* 52:775–782.

Geerts, H., M. De Brabander, and R. Nuydens. 1991. Nanovid microscopy. *Nature (Lond.).* 351:765–766.

Gelles, J., B. J. Schnapp, and M. P. Sheetz. 1988. Tracking kinesin-driven movements with nanometre-scale precision. *Nature (Lond.).* 331:450–453.

Gross, D. J., and W. W. Webb. 1988. Cell surface clustering and mobility of the liganded LDL receptor measured by digital video fluorescence microscopy. *In* Spectroscopic Membrane Probes II. L. M. Loew, editor. CRC Press, Boca Raton, Florida. 19–45.

Heins, Y. I., Z. Katzir, M. A. Shia, and H. F. Lodish. 1990. Oligomeric structure of the human asialoglycoprotein receptor: nature and stoichiometry of mutual complexes containing H1 and H2 polypeptides assessed by fluorescence photobleaching recovery. *J. Cell Biol.* 111:1409–1418.

Jacobson, K., A. Ishihara, and R. Inman. 1987. Lateral diffusion of proteins in membranes. *Annu. Rev. Physiol.* 49:163–175.

Kucik, D. F., E. L. Elson, and M. P. Sheetz. 1989. Forward transport of glycoproteins on leading lamellipodia in locomoting cells. *Nature (Lond.).* 340: 315–317.

Kusumi, A., and J. S. Hyde. 1982. Spin-label saturation-transfer electron spin resonance detection of transient association of rhodopsin in reconstituted membranes. *Biochemistry.* 21:5978–5983.

Kusumi, A., T. Sakaki, T. Yoshizawa, and S. Ohnishi. 1980. Protein-lipid interaction in rhodopsin recombinant membranes as studied by protein rotational mobility and lipid alkyl chain flexibility measurements. *J. Biochem.* 88:1103–1111.

Kusumi, A., Y. Sako, and M. Yamamoto. 1993. Confined lateral diffusion of membrane receptors as observed by single particle tracking (nanovid microscopy): effects of calcium-induced differentiation of epithelial cells. *Biophys. J.* 65:2021–2040.

Lee, G. M., A. Ishihara, and K. A. Jacobson. 1991. Direct observation of Brownian motion of lipids in membranes. *Proc. Natl. Acad. Sci. USA.* 88:6274–6278.

Leunissen, J. L. M., and J. R. De Mey. 1986. Preparation of gold probes. *In* Immuno-Gold Labeling in Cell Biology. A. J. Verkleij and J. L. M. Leunissen, editors. CRC Press, Boca Raton, Florida. 3–16.

Livneh, E., M. Benveniste, R. Prywes, S. Felder, Z. Kam. and J. Schlessinger. 1986. Large deletions in the cytoplasmic kinase domain of the epidermal growth factor receptor do not affect its lateral mobility. *J. Cell Biol.* 103: 327–331.

Luna, E. J., and A. L. Hitt. 1992. Cytoskeleton-plasma membrane interactions. *Science (Wash. DC)* 258:955–964.

Mecham, R. P., L. Whitehouse, M. Hay, A. Hinek, and M. P. Sheetz. 1991. Ligand affinity of the 67-kD elastin/laminin binding protein is modulated by the protein's lectin domain: visualization of elastin/laminin-receptor complexes with gold-tagged ligands. *J. Cell Biol.* 113:187–194.

Metzger, H. 1992. Transmembrane signaling: the joy of aggregation. *J. Immunol.* 149:1477–1487.

Miller, K., M. Shipman, I. S. Trowbridge, and C. R. Hopkins. 1991. Transferrin receptors promote the formation of clathrin lattices. *Cell.* 65:621–632.

Pearse, B. M. F., and R. A. Crowther. 1987. Structure and assembly of coated vesicles. *Annu. Rev. Biochem.* 16:49–68.

Pearse, B. M. F., and M. S. Robinson. 1990. Clathrin, adaptors, and sorting. *Annu. Rev. Cell Biol.* 6:151–171.

Peters, R., and R. J. Cherry. 1982. Lateral and rotational diffusion of bacteriorhodopsin in lipid bilayers: experimental test of the Saffman-Delbrück equations. *Proc. Natl. Acad. Sci. USA.* 79:4317–4321.

Poo, M.-M., and R. A. Cone. 1974. Lateral diffusion of rhodopsin in the photoreceptor membrane. *Nature (Lond.).* 247:438–441.

Qian, H., M. P. Sheetz, and E. Elson. 1991. Single particle tracking (Analysis of diffusion and flow in two-dimensional systems). *Biophys. J.* 60:910–921.

Saxton, M. J. 1987. Lateral diffusion in an archipelago. The effect of mobile obstacles. *Biophys. J.* 52:989–997.

Saxton, M. J. 1989*a*. Lateral diffusion in an archipelago. Distance dependence of the diffusion coefficient. *Biophys. J.* 56:615–622.

Saxton, M. J. 1989*b*. The spectrin network as a barrier to lateral diffusion in erythrocytes. A percolation analysis. *Biophys. J.* 55:21–28.

Saxton, M. J. 1990*a*. The membrane skeleton of erythrocytes. A percolation model. *Biophys. J.* 57:1167–1177.

Saxton, M. J. 1990*b*. The membrane skeleton of erythrocytes: models of its effect on lateral diffusion. *Int. J. Biochem.* 22:801–809.

Saxton, M. J. 1993. Lateral diffusion in an archipelago. Single particle diffusion. *Biophys. J.* 64:1766–1780.

Schnapp, B. J., J. Gelles, and M. P. Sheetz. 1988. Nanometer-scale measurement using video light microscopy. *Cell Motil. Cytoskeleton.* 10:47–53.

Sheetz, M. P., M. Schindler, and D. E. Koppel. 1980. Lateral mobility of integral membrane proteins is increased in spherocytic erythrocytes. *Nature (Lond.).* 285:510–512.

Sheetz, M. P., S. Turney, H. Qian, and E. L. Elson. 1989. Nanometre-level analysis demonstrates that lipid-flow does not drive membrane glycoprotein movements. *Nature (Lond.).* 340:284–288.

Takeuchi, M., H. Miyamoto, H. Komizu, and A. Kusumi. 1992. Atomic force microscopy (AFM) observation of the membrane skeleton network: comparison with electron microscopy. *Cell Struct. Funct.* 17:487.

Tsuji, A., and S. Ohnishi. 1986. Restriction of the lateral motion of band 3 in the erythrocyte membrane by the cytoskeletal network: dependence on spectrin association state. *Biochemistry.* 25:6133–6139.

Tsuji, A., K. Kawasaki, S. Ohnishi, H. Merkle, and A. Kusumi. 1988. Regulation of band 3 mobilities in erythrocyte ghost membranes by protein association and cytoskeletal meshwork. *Biochemistry.* 27:7447–7452.

Ullrich, A., and J. Schlessinger. 1990. Signal transduction by receptors with tyrosine kinase activity. *Cell.* 61:203–212.

Vaz, W. L. C., F. Goodsaid-Zalduondo, and K. Jacobson. 1984. Lateral diffusion of lipids and proteins in bilayer membranes. *FEBS (Fed. Eur. Biochem. Soc.) Lett.* 174:199–207.

Yechiel, E., and M. Edidin. 1987. Micrometer-scale domains in fibroblast plasma membranes. *J. Cell Biol.* 105:755–760.

Zhang, F., B. Crise, B. Su, Y. Hou, J. K. Rose, A. Bothwell, and K. Jacobson. 1991. Lateral diffusion of membrane-spanning and glycosylphosphatidylinositol-linked proteins: toward establishing rules governing the lateral mobility of membrane proteins. *J. Cell Biol.* 115:75–84.